ACS Combinatorial Science

Research Article

pubs.acs.org/acscombsci

High-Throughput Compositional and Structural Evaluation of a $Li_a(Ni_xMn_yCo_z)O_r$ Thin Film Battery Materials Library

Sara Borhani-Haghighi,[†,⊥] Michael Kieschnick,[†,‡,⊥] Yahya Motemani,[†] Alan Savan,[†] Detlef Rogalla,[‡] Hans-Werner Becker,[‡] Jan Meijer,[§] and Alfred Ludwig*[,†,∥]

[†]Institute for Materials, Faculty of Mechanical Engineering, Ruhr-Universität Bochum, Bochum, Germany.

[‡]RUBION, Central Unit for Ion Beams and Radionuclides, Ruhr-Universität Bochum, Bochum, Germany.

[§]Institute for Experimental Physics II, Department of Nuclear Solid State Physics, Leipzig Universität, Leipzig, Germany

[∥]Materials Research Department, Ruhr-Universität Bochum, Bochum, Germany

Supporting Information

ABSTRACT: A $Li_a(Ni_xMn_yCo_z)O_r$ cathode materials library was fabricated by combinatorial magnetron sputtering. The compositional analysis of the library was performed by a new high-throughput approach for Li-content measurement in thin films, which combines automated energy-dispersive X-ray spectroscopy, Deuteron-induced gamma emission, and Rutherford backscattering measurements. Furthermore, combining this approach with thickness measurements allows the mapping of density values of samples from the materials library. By correlating the obtained compositional data with structural data from high-throughput X-ray diffraction measurements, those compositions which show a layered ($R\bar{3}m$) structure and are therefore most interesting for Li-battery applications (for cathode (positive) electrodes) can be rapidly identified. This structure was identified as being most pronounced in the compositions $Li_{0.6}(Ni_{0.16}Mn_{0.35}Co_{0.48})O_2$, $Li_{0.7}(Ni_{0.10}Mn_{0.37}Co_{0.51})O_2$, $Li_{0.6}(Ni_{0.23}Mn_{0.33}Co_{0.43})O_2$, $Li_{0.3}(Ni_{0.65}Mn_{0.08}Co_{0.26})O_2$, $Li_{0.3}(Ni_{0.63}Mn_{0.08}Co_{0.29})O_2$, $Li_{0.4}(Ni_{0.56}Mn_{0.09}Co_{0.34})O_2$, $Li_{0.5}(Ni_{0.45}Mn_{0.13}Co_{0.42})O_2$, and $Li_{0.6}(Ni_{0.34}Mn_{0.14}Co_{0.52})O_2$.

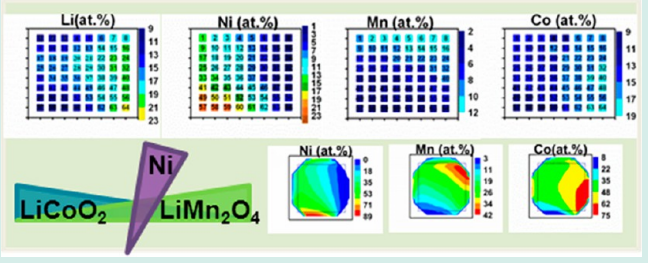

KEYWORDS: *lithium-ion batteries, cathode, combinatorial materials science, high-throughput methods, thin films library, DIGE*

INTRODUCTION

The development of better Li-based batteries requires the optimization of key battery components, that is, the cathode, the anode, and the electrolyte. For both cathode and anode materials development, combinatorial and high-throughput methods have been used.[1−11] Next to investigations based on powders, thin film methods have been used, with the main focus on anode materials such as Si, Sn, Sn-M, and Si-M (M: transition metal).[3−5,12−15] An early combinatorial investigation of Li-ion battery electrode materials was conducted by Watanabe et al. where layered Li−Co−Mn−O powder mixtures were synthesized using a combinatorial robot system.[9] In 2003, Sponge et al. fabricated 64 $Li_xMn_2O_4$-based powder composites by an automated parallel synthesis technique.[11] Extensive research on combinatorial fabrication and characterization of anode materials has been conducted by Dahn et al., who investigated various material systems such as Mo−Sn, Mn−Si−Fe, Si−Al−Mn, and Si−Sn using a combinatorial magnetron sputtering approach and characterized them with a combinatorial electrochemical cell.[3,4,12,13] A survey conducted by Todd et al. on the structural and electrochemical properties of sputtered Sn-M (M = Ti, V, Mn, Cr, Ni, Fe, Co, Cu) thin films showed that the specific capacity of these battery electrodes drops with the increase in M content.[5,14,15]

While anode materials have been already extensively studied with the combinatorial approach, only few studies exist on combinatorial screening of thin film cathode materials. Whitacre et al. fabricated (via sputtering) and characterized $Li_yMn_xNi_{2-x}O_4$ solid-state batteries, and $LiMn_{1.4}Ni_{0.6}O_4$ was identified to possess the highest specific capacity.[10]

A general problem in these combinatorial investigations is the determination of the Li content of the samples within a materials library. While this is not easy for powder materials, it is even more challenging for thin film materials libraries. For nonhigh-throughput approaches, Habrioux et al. presented a non-destructive approach for the characterization of bulk $LiFePO_4$ cathodes, which could be adapted for the measurement of Li-containing films.[16] They used Proton-Induced X-ray Emission (PIXE), Rutherford Backscattering Spectroscopy (RBS), and Proton-Induced Gamma-ray Emission (PIGE). A potential weakness of this approach is that the absolute Li content measurement using PIGE is more fallible in thin films than in bulk samples and needs a complex data analysis. Whitacre et al.[10] used a combination of energy-dispersive X-ray spectroscopy

Received: January 31, 2013
Revised: April 10, 2013
Published: May 22, 2013

(EDX) and RBS measurements, along with Inductively Coupled Plasma Mass Spectrometry (ICP-MS) to measure the Li/Mn ratio. However in this method the signal is retrieved from an area of 2 to 3 cm^2. This measurement area is too large for materials libraries of a practical size, which have significant concentration gradients on such a scale.

The main focus of this paper is to establish a reliable high-throughput method for the compositional analysis of Li-Metal-Oxide thin films. This is based on a combination of the methods EDX, Deuteron Induced Gamma Emission (DIGE), and RBS: further referred to as E-D-R approach. DIGE is used to measure the Li/O ratio in thin film materials libraries of the system $Li_a(Ni_xMn_yCo_z)O_r$ (NMC). NMC was chosen as it is one of the promising cathode materials systems and was fabricated by combinatorial sputtering. The chemical compositions obtained by E-D-R are correlated with structural data from X-ray diffraction (XRD) experiments. As a result we identify compositions with promising structure for battery applications.

RESULTS AND DISCUSSION

E-D-R Methodology for High-Throughput Compositional Analysis of NMC Materials Libraries. Reported composition characterization techniques for thin films are either destructive and unsuitable for material libraries with high composition gradients[10] or not conveniently adaptable to thin film samples.[16] Therefore this paper attempts to establish a suitable methodology for the complete compositional characterization of thin film libraries such as $Li_a(Ni_xMn_yCo_z)O_r$. The combination of EDX, DIGE, and RBS (E-D-R) is proposed as a promising method. An overview of the E-D-R approach is given in Figure 1. First, automated EDX (JEOL JSM 5800 SEM equipped with an Oxford Inca system) was performed on the materials library. The transition metals (M) along with O and Si (from the substrate) were mapped; however, only the distribution of the transition metals, M, across the library was considered in the EDX data analysis. Only the *K* shell signals of the transition metals were used in the EDX data analysis to avoid errors from overlap of the *L* shell signal of the transition metals with the K shell signal of O. The accelerating voltage and measurement time during the EDX measurement were 20 kV and 60 s, respectively. In total 20 × 21 points with step increments of 4.5 mm were measured in the mapping process. The error of the EDX measurement is estimated to be about 1%. The EDX measurement of two identical materials libraries deposited on both Si/SiO_2 and Si substrates yielded also similar results. While O might be measured by EDX with a limited accuracy, Li cannot be quantified with EDX.

Therefore, in a second step DIGE was performed in the center of 64 measurement regions to obtain the content of the light elements (L) in the thin films; the measurement time was ~15 min per measurement region. Because of the low nuclear charge of light elements such as Li and O, they have relatively high reaction cross sections for the reaction with deuterons. Therefore DIGE is especially sensitive to light elements, but cannot be used for heavy elements. DIGE is not depth-sensitive and cannot distinguish between O in the film and in the substrate. Hence it is necessary to perform DIGE measurements on oxide-free substrates, that is, Si(100) with only a native oxide on top. In the DIGE measurement, the samples (20° tilt) were irradiated with a 1 MeV $^2D^{1+}$ beam (beam spot size ~4 mm^2). A gamma spectrum was measured with a HPGe detector at 90° with respect to the beam. A peak at 478 keV results from the reaction $^6Li(d,p\gamma)^7Li$ and a peak at 871 keV results from $^{16}O(d,p\gamma)^{17}O$.[17]

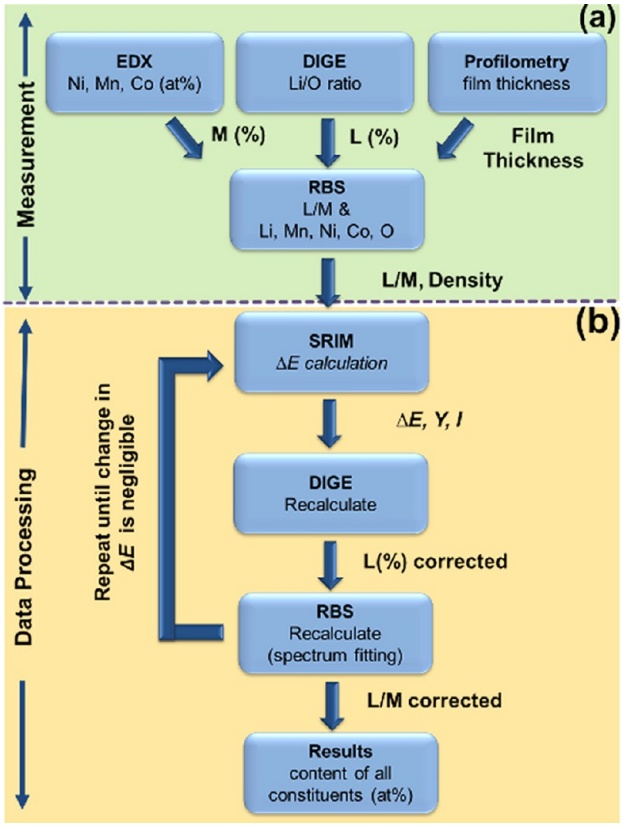

Figure 1. Flowchart illustrating the E-D-R approach. (a) EDX, DIGE, RBS, and profilometry are combined with (b) data processing for composition determination. L and M represent light elements (i.e., Li and O) and transition metals (Ni, Mn, Co) respectively. Δ*E*, *Y*, and *I* represent energy loss calculated for each measurement region, yield for Li or O, and theoretical signal intensity calculated for each measurement region, respectively.

A bulk reference sample with known composition ($Li_4Ti_5O_{12}$) was used to calibrate the ratio of Li and O peaks with respect to each other. Since EDX and DIGE (as used in the E-D-R approach) only yield relative composition values, an additional RBS measurement is needed to determine the L/M ratio and therefore the absolute concentration of each constituent. A 2 MeV $^4He^{1+}$ beam (Cornell geometry, scattering angle 160°, tilt angle 7°) was used for the RBS measurements (beam spot size 1 mm^2). The measured spectra were subsequently fitted using the RBX code.[17] The combined results from these three measurements lead to a preliminary estimate of the composition of the films. However, further data processing is needed to get to accurate values of the content of all constituents of the thin films.

The results from the first step of the E-D-R approach, EDX high-throughput measurements for the elements Mn, Co, and Ni are visualized in Figure 2. Since only Mn, Co, and Ni in these thin films can be measured accurately with EDX, their relative concentrations were calculated with the assumption that the thin film library consists only of these three constituents. The X-ray energies of these transition metals are in the same energy range, therefore the systematic measurement error caused is negligible.

In a second step, the Li/O ratio was determined using DIGE. A typical sample spectrum is shown in Figure 3(a) (red curve), with (b) and (c) showing the peaks of Li and O. The shaded area is the actual gamma peak used for further analysis. The background signal mainly results from Compton scattering of higher energetic γ rays inside the detector and thus varies for different

dx.doi.org/10.1021/co4000166 | ACS Comb. Sci. 2013, 15, 401−409

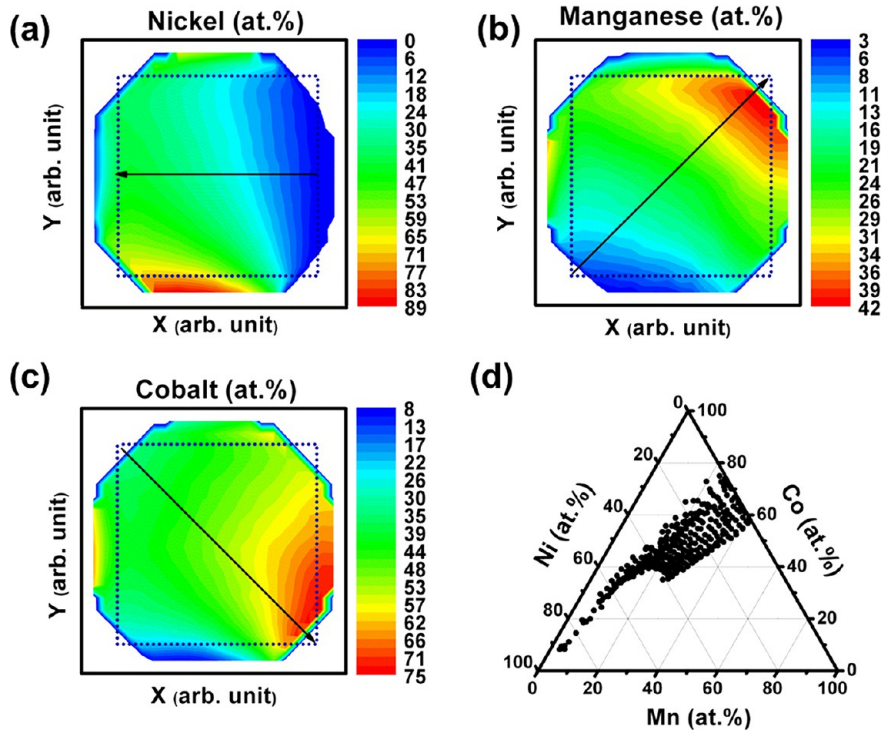

Figure 2. Visualization of EDX results for (a) Ni, (b) Mn, and (c) Co content in a $Li_a(Ni_xMn_yCo_z)O_r$ thin film library on the wafer level. The dotted squares indicate the area of the materials library. Arrows indicate increasing elemental content and the colors blue, green, and red represent low, intermediate and high element contents respectively. (d) A ternary diagram of M.

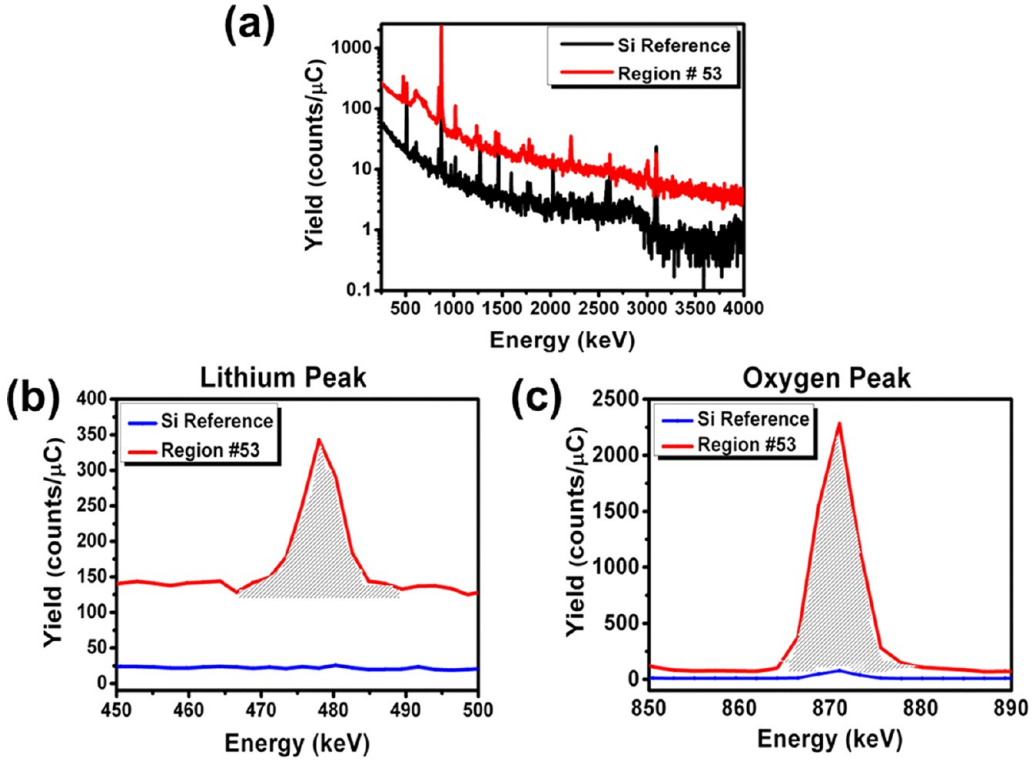

Figure 3. (a) Example of gamma spectra for region #53 and a Si reference (blank). The (b) Li and (c) O signals are shown in detail: the shaded gray area gives the actual peak area.

samples. The detector can only be partially shielded and is influenced by γ rays produced on other parts of the beamline (such as apertures) or the substrate (i.e., native oxide). Therefore an additional reference (blank) measurement as shown in Figure 3 (a) by the black line, had to be performed on an uncoated Si(100) substrate. As Figure 3 (b) and (c) demonstrate, no corrections are necessary for Li, and only minor corrections are needed for the O signal.

dx.doi.org/10.1021/co4000166 | ACS Comb. Sci. 2013, 15, 401−409

Figure 4 shows the results of a RBS measurement in region #53 of the NMC materials library. In the spectrum, three plateaus can be identified which relate to the signal from the transition metals M, O, and the Si(100) substrate. The M signal is detected as a single plateau in the spectrum because of the similar masses of Ni, Mn, and Co. The O plateau does not have a good signal to background ratio, since it is situated on top of the Si substrate signal. Because of its low mass, Li is not detectable as a plateau. Thus only the M plateau was used for fitting the spectra. If the fit is performed only with the M content from EDX (Figure 4, red line), the simulated transition metal signal is too high in comparison to the measured spectrum. Increased amounts of light elements would reduce the probability of scattering on the transition metals and therefore the height of the plateau is reduced as seen in the simulation, blue line in Figure 4. Since the Li/O ratio is known from DIGE, and the ratio of the transition metals to each other is known from EDX, this leaves only the L/M ratio as a free parameter for fitting the spectrum. By an iterative fitting process, this ratio is adjusted until the simulation matches the measured spectrum (Figure 4, green line). This results in a preliminary estimate for the composition of a measurement region which would be correct for a bulk sample.

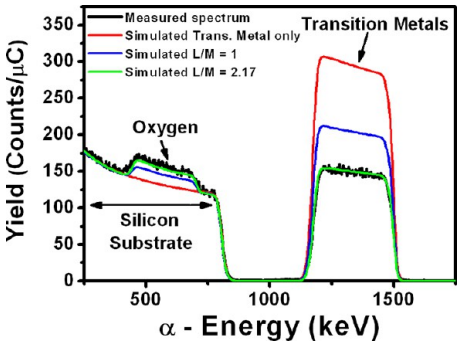

Figure 4. Example RBS measurement of region #53 from the $Li_a(Ni_xMn_yCo_z)O_r$ materials library (black). A simulation taking into account only Ni−Mn−Co ratios excluding Li and O content is shown in red. Another simulation considering a L/M = 1 is depicted in blue. The final simulation for L/M = 2.17, fitting the measured spectrum, is shown in green.

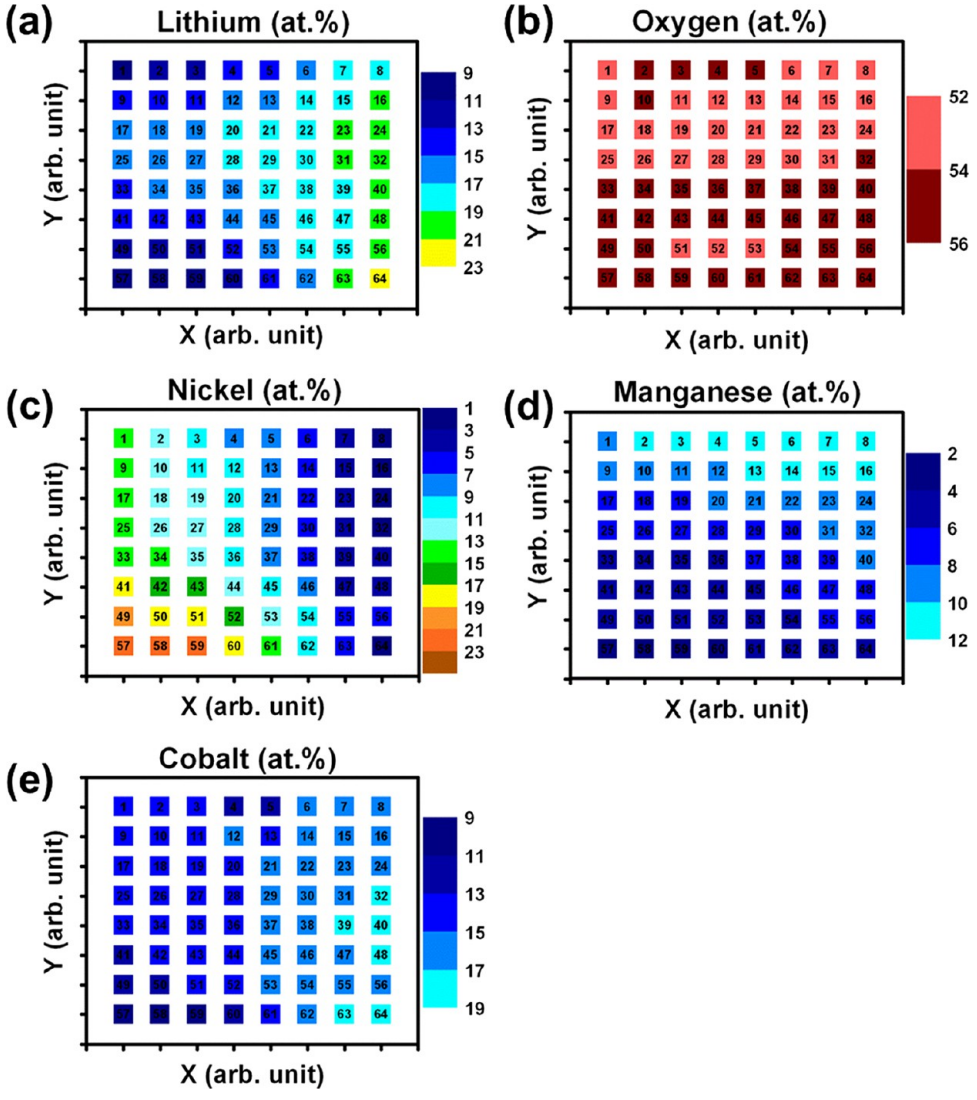

Figure 5. Distribution of elements across the $Li_a(Ni_xMn_yCo_z)O_r$ combinatorial materials library as determined by E-D-R: (a) Li- (b) O-, (c) Ni-, (d) Mn-, (e) Co-content. The color bars indicate the content of each element in at.%.: blue represents the low-end and red the high-end of the measured values. The 64 measurement regions are represented as numbered squares.

dx.doi.org/10.1021/co4000166 | ACS Comb. Sci. 2013, 15, 401−409

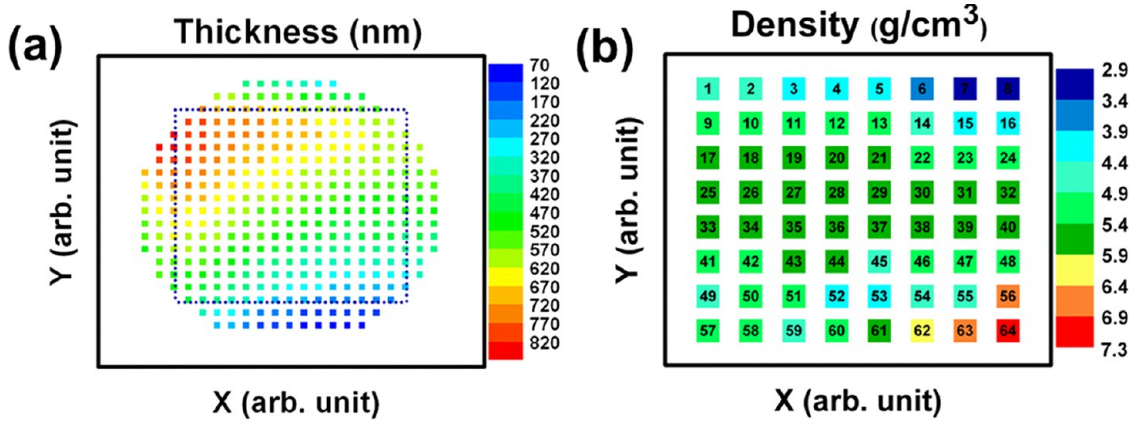

Figure 6. (a) Thickness map across the sample where the dotted box corresponds to the $Li_a(Ni_xMn_yCo_z)O_r$ combinatorial materials library. (b) The numbered squares indicate the 64 (10 mm ×10 mm) measurement regions along with corresponding density. The color bars correspond to the thickness (nm) and density (g/cm^2) respectively: blue represents the low-end and red the high-end of the measured values.

Subsequent iterations as shown in Figure 1 (b) are necessary to sequentially adapt this estimate to the thin films. Because of energy-dependent changes in the reaction cross-section, the expected Li/O signal varies with sample thickness. These thicknesses of the materials library vary from ∼100 to 840 nm and are in an intermediate range for the measurement beam energy, with 30−100 keV energy loss inside the film. For correction of the thickness effects, cross-section data and a fit function (eq 1) from Elekes et al. were used.[18]

$$Y = Y_0 \cdot (E - E_0)^a \quad (1)$$

Y_0, E_0, and a are empirical fit parameters. E is the beam energy, and Y is the resulting thick target yield for Li or O, respectively. Since for this work, only the energy range of up to 1 MeV was relevant, a recalculation of the fit parameters was conducted to focus on that energy range.

Li:

$$Y_0 = 3.715 \times 10^6 N_\gamma/(\text{sr} \times \mu\text{C}); \quad E_0 = 0.1472 \text{ MeV}; \quad a = 7.62$$

O:

$$Y_0 = 9836 N_\gamma/(\text{sr} \times \mu\text{C}); \quad E_0 = -0.56 \text{ MeV}; \quad a = 10.96$$

The signal intensity, I, from each measurement region can then be calculated by eq 2.

$$I = Y(1 \text{ MeV}) - Y(1 \text{ MeV} - \Delta E) \quad (2)$$

For each sample the Y values for O and Li can be obtained from eq 1. The energy loss ΔE inside each measurement region was calculated via SRIM 2008 using the preliminary composition data obtained before.[19] Using this, the fit of the RBS spectra was slightly adjusted, and the final sample composition was determined.

Because of statistical fluctuations in the measurement signal as well as in the Compton background, the DIGE analysis shows count statistic error of up to 10%. The systematic error of the applied thickness correction is assumed to be ∼5% because of imperfections in the gamma yield data as well as in the fit function used for this correction. This leads to a measurement error of ∼15% for the Li/O ratio. However, because of a limited effect of the L composition on the RBS analysis, the absolute M concentration analysis is not heavily affected by different Li/O ratios (15% error in the Li/O ratio equals ∼1 atomic % systematic error in the absolute M concentration). The accuracy of the absolute measurement of M is also limited by the accuracy of EDX (which could be improved by using appropriate standards) as well as the accuracy of the beam current measurement during RBS and can be estimated as ∼5%.

The RBS measurements show that the M/O ratios in the thin film $Li_a(Ni_xMn_yCo_z)O_r$ library vary between 0.5 and 0.7 and the Li/O ratios between 0.2 and 0.5. The variation of the O-content across the materials library is not significant (52−55 at.%). The Co distribution across the library is 10−18 at. %, while it is 3−11% for Mn, 2−19% for Ni, and 10−21% for Li. The distribution of each element across the materials library as determined by E-D-R is shown in Figure 5.

Furthermore, it is also possible to calculate the mean densities of all thin film samples, since RBS spectra also contain information on the areal densities. For this, the film thickness data obtained by profilometry was used. The measurement error for these densities is estimated to be 10%. However, it has to be stressed that the measured density is a mean value for the film at each measurement region. A map of thickness and density across the materials library is shown in Figure 6 (a) and (b) respectively. Since not all measurement regions were fully characterized, the concentrations and densities of the nonmeasured regions were calculated using a two-dimensional linear interpolation and extrapolation.

Density is an important value for thin film electrode materials. To determine the charge or applied current for galvanostatic measurements, the mass of active material has to be known. For thin films, even-though the geometry and hence the volume can be precisely calculated, the mass is usually derived from theoretical densities which exclude factors such as film porosity, introducing what can be a significant error. Knowledge of the correct value of density at each region across the library allows for a more accurate electrochemical measurement. The densities determined for the measurement regions across the library vary from 4 to 5.5 g/cm^3; however in measurement region #64, the density reaches the maximum value of 7.3 g/cm^3.

High-Throughput Structural Evaluation of a $Li_a(Ni_xMn_yCo_z)O_r$ Thin Film Library. After having determined the compositions in the NMC library using the E-D-R approach, and using automated XRD measurements for the determination of structural data, composition-structure relations in the library

dx.doi.org/10.1021/co4000166 | ACS Comb. Sci. 2013, 15, 401−409

can be established. The aim is to identify compositions showing a layered structure ($R\bar{3}m$). XRD spectra of the annealed materials library were measured at 64 regions, corresponding to the areas analyzed by E-D-R. Four major Bragg diffraction peaks were observed at 2θ values of approximately 19°, 37°, 45°, and 65°, corresponding to (003), (101) along with (012)/(006), (104), and (110) reflections of the layered hexagonal structure ($R\bar{3}m$) respectively, where the "/" sign indicates peak splitting. Figure 7(a) shows a color-coded map summarizing all the observed

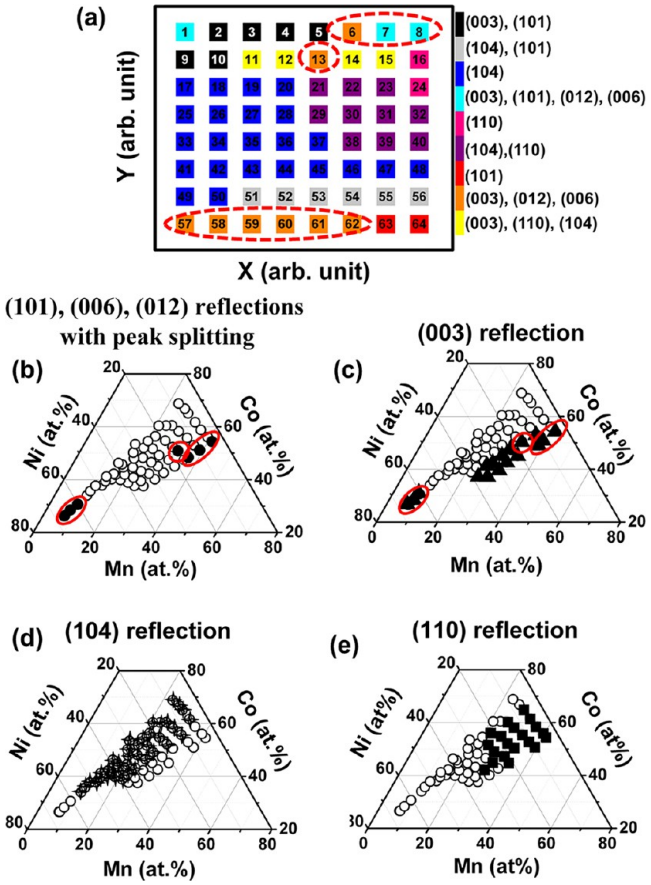

Figure 7. Color map indicating key diffractions observed in each measurement region across the NMC library, the 64 measurement regions are represented as numbered squares (a). Correlation of composition with (b) (101), (012), (006), (c) (003), (d) (104), and (e) (110) reflections of the layered ($R\bar{3}m$) structure are shown. The symbol "○" denotes measured regions which do not show the corresponding diffraction. The regions with highest possibility of having the layered structure are circled in red.

reflections from the materials library. The correlation between the XRD reflections and the composition is shown in Figure 7 (b), (c), (d) and (e).

Good cation ordering in the hexagonal structure can be confirmed by a higher intensity of the (003) peak compared to the (104) peak.[20] Another confirmation of the presence of the layered hexagonal structure is a distinct peak splitting between (006) and (012), which is the result of the distortion of the oxygen sublattice in the $R\bar{3}m$ structure in the hexagonal *c*-direction.[20,21] Partial interchange of the occupancy of Li and transition metal oxides among the *3b* (i.e., Li) sites and *3a* (i.e., transition metal) sites results in cation mixing. This cation mixing results in the absence of distortion in the hexagonal *c*-direction and causes the (006)/(012) peaks to merge into single peaks.[21−24]

The (104) reflection of the $R\bar{3}m$ is present almost throughout the entire library, the exceptions being in regions where the (003) reflection was most pronounced. As Figure 7 (a) shows, measurement regions #1, #7, #8 (cyan) and measurement regions #6, #13 and #57−#62 (orange) show the (003) reflection at $2\theta \approx 19°$ along with a distinct peak splitting of (006) and (012) at $2\theta = 37°$. These observations are in agreement with reports by Yoshio et al. where Co-doping of $LiMn_xNi_{1-x}O_2$ stabilized the layered hexagonal structure.[25] However, in this study, the (003) reflection in the XRD spectra of these measurement regions is not the most intense peak compared to the other reflections. From this it is still likely that the hexagonal layered structure ($R\bar{3}m$) is present in these measurement regions.

XRD spectra of measurement regions #1 and #6 are shown as an example in Figure 8(a). In measurement regions #1, #8, #57, and #64, a peak at $2\theta \approx 41−42°$ corresponding to the (200) reflection of the cubic-NaCl type-structure ($Fm\bar{3}m$),[26] indicated by "•", is observed (Figure 8 (a) and (d)). Measurement regions #1 and #8 also demonstrate the (003), (101), and (012)/(006) reflections of the layered hexagonal ($R\bar{3}m$) structure. Coexistence of the hexagonal layered structure and cubic structure in these samples can be concluded. These sample regions are shown by cyan color in Figure 7 (a). However, the XRD spectrum of measurement region #7 ("cyan" color group) shows the presence of only a hexagonal layered structure. Figure 8(b) and (c) demonstrate XRD spectra of selected measurement regions having reflections at $2\theta \approx 65°$ and $2\theta \approx 45°$. Some of the dark blue color-coded measurement regions shown in Figure 8(a) with reflections at $2\theta \approx 45°$ ((104) reflection)) show a "shoulder" as marked by "*" in Figure 8(c). This shoulder could be due to the coexistence of (400) reflection of cubic ($Fd\bar{3}m$) phase along with the (104) reflection of the hexagonal layered structure.[27] Another possibility for this shoulder could be peak splitting. It is known that the (104) reflection in $R\bar{3}m$ is a 3-fold degenerate of (104), ($01\bar{4}$) and ($1\bar{1}4$) reflections and is observed as one reflection splitting of the other two overlapped reflections. This phenomenon is a result of basal plane distortions in the hexagonal layered structure.[28] However when there are basal plane distortions in the hexagonal layered ($R\bar{3}m$) structure, peak splitting of the (110) reflection should also be observed.[28] Inspection of the (110) reflection of the ($R\bar{3}m$) phase shows no sign of peak-splitting (Figure 8(b) and (c)); leading to the conclusion that basal plane distortion in these films is not significant.

If the material possesses a layered structure, the *r* value for oxygen in $Li_a(Ni_xMn_yCo_z)O_r$ can be set to 2.[10] Accordingly, the compositions corresponding to each of the measured regions are listed in Supporting Information, Tables S1 and S2. Correlation of composition and structural analysis demonstrates that the compositions $Li_{0.6}(Ni_{0.16}Mn_{0.35}Co_{0.48})O_2$, $Li_{0.7}(Ni_{0.10}Mn_{0.37}Co_{0.51})O_2$, $Li_{0.6}(Ni_{0.23}Mn_{0.33}Co_{0.43})O_2$, $Li_{0.3}(Ni_{0.65}Mn_{0.08}Co_{0.26})O_2$, $Li_{0.3}(Ni_{0.63}Mn_{0.08}Co_{0.29})O_2$, $Li_{0.4}(Ni_{0.56}Mn_{0.09}Co_{0.34})O_2$, $Li_{0.5}(Ni_{0.45}Mn_{0.13}Co_{0.42})O_2$, and $Li_{0.6}(Ni_{0.34}Mn_{0.14}Co_{0.52})O_2$ have the layered hexagonal structure. Hence these compositions are promising candidates for Li-ion battery cathode materials. Further electrochemical analysis is necessary to confirm this, and is the subject of continuing investigations.

dx.doi.org/10.1021/co4000166 | *ACS Comb. Sci.* 2013, 15, 401−409

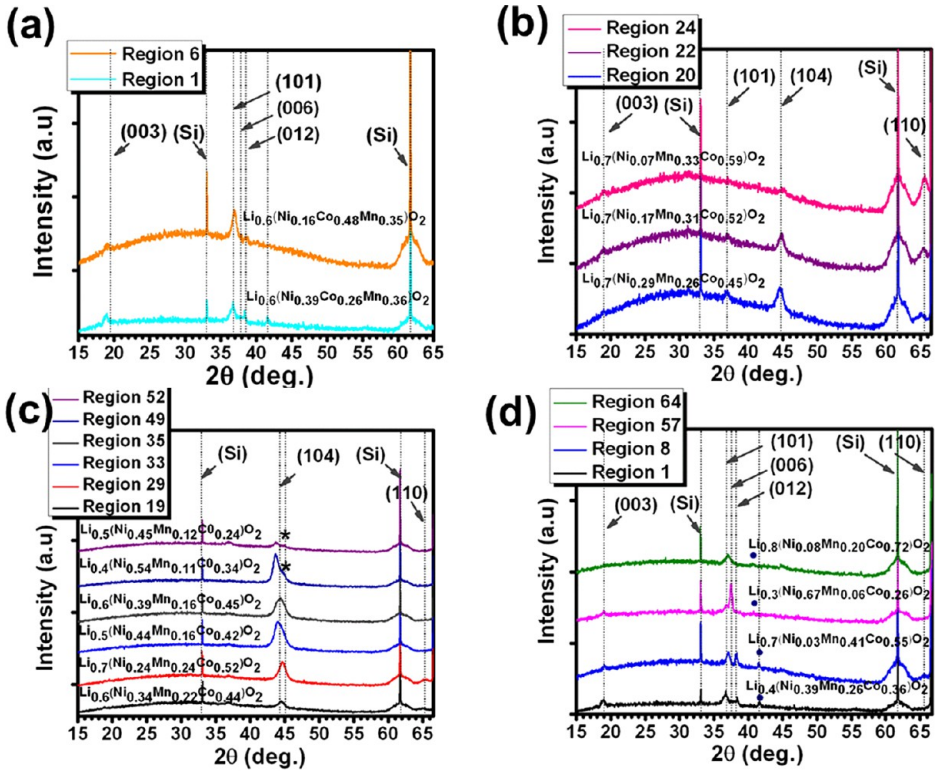

Figure 8. XRD patterns of selected measurement regions in the library. (a) regions indicating the hexagonal layered structure with distinct peak splitting observed at $2\theta = 37°$, (b) example of diffraction patterns of some measurement regions with the (110) reflection at $2\theta = 65°$, (c) some diffraction patterns of measurement regions with reflections at $2\theta = 44–45°$; peak-shoulders are shown with *. (d) In measurement regions #1, #8, #57, and #64 a peak belonging to (200) reflection of $Fm\bar{3}m$ cubic structure, (indicated by blue solid circles) at $2\theta \approx 42°$ is observed along with previously mentioned reflections of hexagonal layered structure ($R\bar{3}m$).

CONCLUSION

$Li_a(Ni_xMn_yCo_z)O_r$ thin film combinatorial libraries were fabricated by magnetron sputtering. A high-throughput approach, E-D-R, for Li-content measurement was introduced. High-throughput study of the structural evolution across the composition spread demonstrated that small changes in transition metal content significantly affect the materials' structure. A layered hexagonal structure was observed for several compositions (making them possible candidates for cathode materials).

EXPERIMENTAL PROCEDURES

Fabrication and Structural Characterization of Materials Libraries. NMC thin film materials libraries were fabricated using a combinatorial sputter system (AJA International) similar to the system described by Dahn et al.[29] The system had a typical base pressure of approximately 2.6×10^{-6} Pa prior to deposition. The sputter chamber is equipped with a 40 cm diameter water-cooled turn-table (rotation speed 18 rpm) with 5 subtables (76 mm ×76 mm), which enable the simultaneous fabrication of 5 identical libraries. Continuous composition spread materials libraries were fabricated using commercial, 2-in. diameter, compound targets of $LiCoO_2$, and $LiMn_2O_4$ (99.9% pure, AJA International, U.S.A.) along with an elemental Ni target (99.9% pure, K.J. Lesker, U.K.). The deposition atmosphere was 99.9999% pure Ar with a flow rate of 30 sccm and a working pressure of 2 Pa. The formation of wedge-type films is achieved with masks in front of each target.[29] The materials libraries of this investigation were deposited by approximately 8640 repetitions of 3 wedge type layers, leading to a thin film materials library with thickness varying from ~100 nm in the thin end to ~840 nm in the thick end. $LiCoO_2$ and $LiMn_2O_4$ were deposited as opposing wedges, whereas a Ni wedge was deposited perpendicular to the other two wedges. In individual terms, the $LiCoO_2$, $LiMn_2O_4$, and Ni wedges have thickness ranging from 30 nm, 25 nm, and 10 nm in the thin end and 610 nm, 290 nm, and 135 nm in the thick end, respectively. Oxides were deposited with 200 W rf. Ni was sputtered at 20 W dc. The use of a Ni target instead of a compound target (e.g., $LiNiO_2$) was due to limitations on the number of available rf power supplies for this sputter system. The minimum dc power at which Ni could be kept ignited throughout the sputtering process was 20 W; even at this low power the Ni deposition rate is higher than that of $LiMn_2O_4$ and $LiCoO_2$, leading to the observed distribution of elements shown in Figure 2, with some compositions showing high Ni content. Two types of substrates were used: (a) 100 mm diameter Si(100) wafer with native oxide (for RBS and DIGE measurements), (b) 100 mm diameter Si(100) wafer with a 1.5 μm thick SiO_2 layer acting as a diffusion barrier (for materials libraries to be postdeposition annealed). A materials library consists of the 76 mm × 76 mm area of the substrate directly in front of the sputter masks. Si/SiO_2 substrates patterned with 342 crosses by a lift-off process (photolithography, photoresist spinning, exposure, and development) were used for thickness measurements. After film deposition, the photoresist was stripped in acetone and isopropanol, and the step heights of the 342 crosses were measured with an automated XP2 stylus profilometer. The NMC library, deposited on patterned Si/SiO_2 substrates for thickness measurements, was annealed in air at 600 °C for 5 h. After annealing, the 64 measurement regions (each 10 mm × 10 mm,

dx.doi.org/10.1021/co4000166 | ACS Comb. Sci. 2013, 15, 401–409

see Figure 7 (a)) were characterized by automated XRD measurements (Bragg−Brentano), using a Panalytical X'pert Pro-MRD system with a Cu target X-ray tube. The materials library was placed on an x-y translation stage, and the measurements and movement operations were sequentially programmed. The diffraction patterns were collected between 2θ angles of 10° to 90° with a step size of 0.026° and a time per step of 100 s. A PIXcel solid state detector (allowing data to be gathered from 255 points simultaneously) was used and therefore a typical measurement time was 20 min per measurement region in the library. Visualization and data management of the diffraction data were conducted using the "XRD-suite" software.[17] Pearson's crystal structure database for inorganic compounds was used as a reference source for phase analysis.[30]

■ ASSOCIATED CONTENT

Supporting Information

Detailed description of composition of all 64 measurement regions and composition structure correlation (Tables S1 and S2). This material is available free of charge via the Internet at http://pubs.acs.org.

■ AUTHOR INFORMATION

Corresponding Author

*E-mail: alfred.ludwig@rub.de. Phone: +49 (0)234-32-27492. Fax: +49 (0)234-32-14409.

Author Contributions

⊥S.B-H and M.K have contributed equally to this work. The manuscript was written through contributions of all authors. All authors have given approval to the final version of the manuscript.

Funding

This work has been funded by DFG within priority program SPP 1473 (WeNDeLIB) and SFB TR 87. Also support from Materials Research Department of RUB is acknowledged.

Notes

The authors declare no competing financial interest.

■ ACKNOWLEDGMENTS

The authors would also like to thank Mr. Sven Hamann for fruitful discussions.

■ REFERENCES

(1) Bonakdarpour, A.; Hewitt, A. C.; Hatchard, T. D.; Fleischauer, M. D. Combinatorial synthesis and rapid characterization of $Mo_{1-x}Sn_x$ ($0 \leq x \leq 1$) thin films. *Thin Solid Films* **2003**, *440*, 11−18.

(2) Chang, S. K.; Kim, H. J.; Hong, S. T. A new lithium-copper-iron-oxide as a negative electrode material for lithium-ion batteries. *J. Power Sources* **2003**, *119−120*, 69−75.

(3) Beattie, S. D.; Dahn, J. R. Combinatorial electrodeposition of ternary Cu-Sn-Zn alloys. *J. Electrochem. Soc.* **2005**, *152*, C542−C548.

(4) Fleischauer, M. D.; Hatchard, T. D.; Bonakdarpour, A.; Dahn, J. R. Combinatorial investigations of advanced Li-ion rechargeable battery electrode materials. *Meas. Sci. Technol.* **2005**, *16*, 212−220.

(5) Todd, A. D. W.; Mar, R. E.; Dahn, J. R. Combinatorial study of tin-transition metal alloys as negative electrodes for lithium-ion batteries. *J. Electrochem. Soc.* **2006**, *153*, A1998−A2005.

(6) Liao, P.; MacDonald, B. L.; Dunlap, R. A.; Dahn, J. R. Combinatorially prepared $[LiF]_{1-x}Fe_x$ nanocomposites for positive electrode materials in li-ion batteries. *Chem. Mater.* **2008**, *20*, 454−461.

(7) Zhou, Y.; Wu, X.; Fu, Z. Combinatorial investigations of Co-LiF and Co-Li_3N nanocomposite as new lithium storage material. In *Proceedings of the Nanoelectronics Conference*, 2008, 2nd IEEE International, pp 69−73.

(8) Carey, G. H.; Dahn, J. R. Combinatorial synthesis of mixed transition metal oxides for lithium-ion batteries. *ACS Comb. Sci.* **2011**, *13*, 186−189.

(9) Yanase, I.; Ohtaki, T.; Watanabe, M. Application of combinatorial process to $LiCo_{1-x}Mn_xO$ ($0 < x < 0.2$) powder synthesis. *Solid State Ionics* **2002**, *151*, 189−196.

(10) Whitacre, J. F.; West, W. C.; Ratnakumar, B. V. A Combinatorial Study of $Li_yMn_xNi_{2-x}O4$ Cathode Materials Using Microfabricated Solid-State Electrochemical Cells. *J. Electrochem. Soc.* **2003**, *150*, A1676−A1683.

(11) Spong, A. D.; Vitins, G.; Guerin, S.; Hayden, B. E.; Russell, A. E.; Owen, J. R. Combinatorial arrays and parallel screening for positive electrode discovery. *J. Power Sources* **2003**, *119−121*, 778−783.

(12) Beattie, S. D.; Dahn, J. R. Masked electrodeposition of a composition-spread library of Sn-Zn alloys onto a 64-channel combinatorial cell plate. *J. Electrochem. Soc.* **2005**, *152*, C549−C551.

(13) Li, J.; Dahn, H. M.; Sandefrson, R. J.; Todd, A. D. W.; Dahn, J. R. Impact of rare earth additions on transition metal oxides as negative electrodes for lithium-ion batteries. *J. Electrochem. Soc.* **2008**, *155*, A975−A981.

(14) Todd, A. D. W.; R.E. Mar, R. E.; Dahn, J. R. Tin-transition metal-carbon systems for lithium-ion battery negative electrodes. *J. Electrochem. Soc.* **2007**, *154*, A597−A604.

(15) Todd, A. D. W.; Ferguson, P. P.; Fleischauer, M. D.; Dahn, J. R. Tin-based materials as negative electrodes for Li-ion batteries: Combinatorial approaches and mechanical methods. *Int. J. Energy Res.* **2010**, *34*, 535−555.

(16) Habrioux, A.; Surblé, S.; Berger, P.; Khodja, H.; D'Affroux, A.; Mailey, S.; Gutel, T.; Patoux, S. Nuclear microanalysis of lithium dispersion in LiFePO4 based cathode materials for Li-ion batteries. *Nucl. Instrum. Methods Phys. Res. B* **2012**, *290*, 13−18.

(17) Kótai, E. Computer methods for analysis and simulation of RBS and ERDA spectra. *Nucl. Instrum. Methods Phys. Res. B* **1994**, *85*, 588−596.

(18) Elekes, Z.; Kiss, A. Z.; Biron, I.; Calligaro, T.; Salomon, J. Thick target γ-ray yields for light elements measured in the deuteron energy interval of 0.7−3.4 MeV. *Nucl. Instrum. Methods Phys. Res. B* **2000**, *168*, 305−320.

(19) Ziegler, J. F.; Biersack, J. P. *SRIM-2008*, programs to calculate Stopping Power and Range of Ions in Matter; *International Atomic Energy Agency (IAEA)*, 2008.

(20) Shaju, K. M.; Subba Rao, G. V.; Chowdari, B. V. R. Performance of layered $Li(Ni_{1/3}Co_{1/3}Mn_{1/3})O_2$ as cathode for Li-ion batteries. *Electrochim. Acta* **2002**, *48*, 145−151.

(21) Tang, A.; Huang, K. Electrochemical properties and structural characterization of layered $Li_xNi_{0.35}Co_{0.3}Mn_{0.35}O_{2+\delta}$ cathode materials. *Mater. Sci. Eng., B* **2005**, *122*, 115−120.

(22) Choi, J.; Manthiram, A. Factors influencing the crystal chemistry of chemically delithiated layered HNi1−$MnCoO_2$. *J. Mater. Chem.* **2006**, *16*, 1726−1733.

(23) Li, J.; Zhang, Z. R.; Guo, X. J.; Yang, Y. The studies on structural and thermal properties of delithiated $Li_xNi_{1/3}Co_{1/3}Mn_{1/3}O_2$ as a cathode material in lithium ion batteries. *Solid State Ionics* **2006**, *177*, 1509−1516.

(24) Lu, Z.; Beaulie, L. Y.; Donaberger, R. A.; Thomas, C. L.; Dahn, J. R. Synthesis, Structure, and Electrochemical Behavior of Li-$(Ni_xLi_{1/3-2x/3}Mn_{2/3-x/3})O_2$. *J. Electrochem. Soc.* **2002**, *149*, A778−A791.

(25) Yoshio, M.; Naguchi, H.; Itoh, J.; Okada, M.; Mouri, T. Preparation and properties of $LiCo_yMn_xNi_{1-x-y}O_2$ as a cathode for lithium ion batteries. *J. Power Sources* **2000**, *90*, 176−181.

(26) Johnston, W. D.; Sestrich, D. E. The preparation and Crystallography and magnetic properties of $Li_xCo_{1-x}O$ System. *J. Phys. Chem. Solids* **1958**, *7*, 1−13.

(27) Gryffroy, D.; Van Den Berghe, R. E. Cation distribution, cluster structure and ionic ordering of the spinel series $Li_{0.5-y}Mg_yMn_{1.5}O_4$. *J. Phys. Chem. Solids* **1992**, *53*, 777−784.

(28) Reimers, J. N.; Dahn, J. R. Electrochemical and In Situ X-Ray Diffraction Studies of Lithium Intercalation in Li_xCoO_2. *J. Electrochem. Soc.* **1992**, *139*, 2091−2097.
(29) Dahn, J. R.; Trussler, S.; Hatchard, T. D.; Bonakdarpour, A.; Mueller-Neuhaus, T. D.; Hewitt, K. C.; Fleischauer, M. D. Economical Sputtering System To Produce Large-Size Composition-Spread Libraries Having Linear and Orthogonal Stoichiometry Variations. *Chem. Mater.* **2002**, *14*, 3519−3523.
(30) Villars, P.; Cenzual, K. *Pearson's Crystal Data: Crystal Structure Database for Inorganic Compounds*; ASM International: Materials Park, Ohio, U.S.A.

NOTE ADDED AFTER ASAP PUBLICATION

This paper was published on the Web on June 5, 2013, with an error in Figure 3. The corrected version was reposted on July 5, 2013.